New crystal structures of 2D Janus-type transition metal dichalcogenides

Pavel N. Gavryushkin [*1,2,3], Nursultan Sagatov[2], Ekaterina V. Sukhanova[1], and Zakhar I. Popov[1]

[1]*Emanuel Institute of Biochemical Physics of Russian Academy of Sciences, 4 Kosygin Street, Moscow, 119334, Russian Federation*
[2]*Sobolev Institute of Geology and Mineralogy, Siberian Branch of Russian Academy of Sciences, prosp. acad. Koptyuga 3, 630090 Novosibirsk, Russian Federation*
[3]*Novosibirsk State University, Pirogova 2, Novosibirsk 630090, Russian Federation*

Abstract

1. Проведены предсказания и обнаружено несколько новых структур, существенно отличащихся от ранее известных H и T

2. Предсказанные структуры характеризуются динамической стабильностью, однако энтальпии их образования выше энтальпий H и T структур.

3. С помощью автоматизированных топологических алгоритмов проведён поиск топологических аналогов. Все структуры, включая fxt и fes характеризуются уникальными топологическими типами и не имеют структурных аналогов в ICSD. Исключение составляет horH структура, характеризующаяся той же топологией, что и T-структура.

Introduction

Transition metal dichalcogenides (TMDs) represent a wide family of materials consisting of transition metal (TM: group IV, V or VI) surrounded by chalcogen atoms (Ch: S, Se or Te). TMDs crystallize in four main structural types including CdI2, MoS2 and FeS2 in pyrite-type and less frequently observed marcasite-type crystal structures [ссылка]. The first two structural types are characterized by the layered structures with Ch-TM-Ch sandwiches bonded with each other

---

*Electronic address: `gavryushkin@igm.nsc.ru`, `p.gavryushkin@g.nsu.ru`; Corresponding author

by the weak Van-der-Waals bonds and, therefore, the crystals can be exfoliated into individual stable layers [1]. These quasi-2D sandwiches attract considerable attention due to their wide range of properties [2–6]. Particularly the TMDs with TMCh2 stoichiometry can act as semiconductors [7], metals [8], semimetals [9,10] or superconductors [11,12] which make family of TMDs suitable for a lot of applications. At ambient conditions TMCh2 (TM=Mo,W, Ch=S,Se) crystallize in the archetype of molybdenite structure (MoS2) which consists of close-packed layers of chalcogen atoms placed exactly one under another along c-axis and TM atoms occupied the center of trigonal prismatic cavities located between the layers of chalcogen atoms. Different stacking of such 2D layers produce different polytypes. If the stacking repetition is reproduced through each two layers the structure has hexagonal symmetry and according to Ramsdell notation is denoted as 2H-polytype (in this case isolated monolayers are denoted as H-phase) [13]. If one layer of chalcogen atoms shift to be placed in triangular holes the coordination polyhedron changes from trigonal prism to the octahedron and the structure with CdI2 archetype is formed. Because of trignaly symmetry of TMDs monolayers, this structure can be designated as T-phase [13]. Depending on the exact chemical composition of the TMD monolayer one of 1H or 1T phase is thermodynamically stable [14]. For example in the case of TM=Mo, W and Ch=S, Se, Te T-phase is less energetically favorable than H-phase with the same chemical composition, however T structure can be stabilized, for example, by intercalation [15,16], by deformation [17] or surface functionalization [18,19]. Vanadium atom is of separate notice because at ambient conditions it does not produce dichalcogenides [20,21]. VSe2 is known in the form of 2H structure with additional V atoms located in the centers of empty trigonal prisms between the sandwiches and have the composition of Se2V1.005.

Recently a new subclass of TMD - so-called Janus structures (Ch1TMCh2) attracts significant interest. The top-layer of chalcogen atoms (Ch1) of the H-MoCh12 (Ch1 = S, Se) monolayer was successfully changed on the layer of Ch2 atoms and the formation of Janus MoSSe structure was observed experimentally [22,23]. The opportunity to change the top layer of atoms opens an additional degree of freedom to manipulate the properties of TMDs. Janus TMDs have structural symmetry breaking [24,25] resulting in Rashba spin splitting [26] and transverse dipole moment leading to large piezoelectricity [27,28]. The TMD's Janus structures have a lot of potential applications for example in water-splitting [29,30] or hydrogen evolution reaction [31,32]. Theoretical investigations show that, as in the case of pristine monolayers, Janus TMDs with different chemical compositions can be thermodynamically stable in a stable in H and T phases typical for stoichiometric TMDs, however on the other side a non-equivalent structure in the transverse direction may lead to the stabilization of new phases which are not typical for stoichiometric TMDs. This encourages us to search for some new possible Janus TMDs phases.

In the present work, we proposed new Janus TMDs structures having sufficiently different geometry and topology from famous T and H phases and investigated their stability. Using topological analysis we analyzed the uniqueness of the found structures and investigated the possibility of their experimental

synthesis.

Comment. fes structure denoted as S-MS2 in [?], from square. fxt structure denoted as H' in [?]. Similarly there is T' – deformed T-phase. We can follow this notation, designating our phases by symmetry with addition of '.

1 Methods

The search for the lowest-enthalpy monolayer structures of XMY composition was performed using evolutionary algorithms implemented in the USPEX program package [33–35] and the random sampling method implemented in the AIRSS software [36, 37] at various pressures of 50, 100, 200, 300, and 400 GPa.

The crystal structure search within USPEX program was performed in fixed composition mode with 2–6 formula units per unit cell. The number of structures in the first generation of the calculations was equal to 180. 50% of the structures with the lowest enthalpy were selected after the optimization and then used to produce the next generation. A new generation was produced as follow: 50% of all structures were generated by heredity, 10% – by atomic mutation, 10% — by lattice mutation, and 30% — randomly. In average, 40–47 generations were produced and relaxed. Using AIRSS program about 5000–6000 structures were randomly generated and optimized for compounds with 4 and 6 formula units per unit cell and structures with the lowest enthalpy were selected.

The total energies and forces were calculated by solving the Schrödinger equation based on projector augmented plane-wave implementation [38] of density functional theory (DFT) using the VASP program package [39, 40]. Exchange correlation effects were treated in the generalized gradient approximation (GGA) with Perdew-Bürke-Ernzerhof scheme [41].

In all crystal structure prediction calculations medium-quality optimization was performed using the conjugate gradient method [ссылка]. The energy cutoff of plane waves was set to 420 eV and 700 eV for the intermediate structures and then for the most promising of them. The first Brillouin zone was sampled according to Monkhorst-Pack scheme [42] with the density of k-point being equal to 0.5 Å^{-1} and 0.2 Å^{-1}, respectively.

To study a dynamic stability of predicted structures phonon dispersion spectra were calculated within the PHONOPY code [43]. We used VESTA program for crystal structures visualization [44].

2 Results

2.1 Similarity and differences of H, T, fxt and fes structures

Although H and T structures are characterized by different coordination polyhedrons, they are similar in the manner of their interconnection. The H structure

consists of trigonal prisms MoS6 (MoS3Se3 for Janus structures), and T structure – of the octahedra of the same composition (Figure1). Each trigonal prism share all three vertical edges with the neighboring prisms and does not share any faces. As the result, each vertice and each vertical edge of the trigonal prism is common for three prisms (Figure 1). Similarly in T structure, each octahedron share all edges inclined to the plane of sulphur atoms with neighbouring octahedra, and each vertice is common for three octahedra (Figure 1). Bond valence of Mo–S bond is nearly equal to $+4/6$ and there are necessary three such a bonds to compensate negative charge of 2^-i of the suphur atom. The interconnection through the edges but provides the longer distance between high-chargeed Mo4+ ions in comparison with interconnection through the faceing, thus reducing the energy of Couloumb interaction.

The recently found fes and fxt structures are also characterised by trigonal prismatic coordination. However, in these structure prisms are connected not only through edges but also through the faces. The whole structure can be constructued from the two edge-connected trigonal prisms (Figure ??b). As the result, the enthalpis of fxt and fes structures are higher than that of H structure, in full accordance with the Pauling rule [?]. In fxt and fes structures, as well as in H and T structures, each at sulphur are connected to three Mo atoms in fxt and fes structure, providing the local charge balance.

H and T structures provide the most homogenic distribution of sulphur and Mo atoms. Both Mo and S nets consists of the geometrically equal triangular loops. Eadge-sharing interconnection of trigonal prisms realised in fxt and fes structures inevitably results in the appearance of the cavities bigger than that in H and T structures. In fes structure the cavities have the form of the slightly compressed cube (Figure ??). The volume of these cavities is almost two times larger than the volume of the cavities in H structure (38.8 against 17.7 Å^3). In casse of fxt structure, the volume of hexagonal cavities (Figure ?? is almost 8 times larger than in H structure (137.8 against 17.7 Å^3). In contrast to trigonal prisms, the face-sharing of the right octahedra seems to be problematic for quasi 2D structure, as it is results in the deviation from the flat arrangement (Figure??b). However, as it will be shown below, the dynamically stable structures with face sharing deformed octahedra can be also produced.
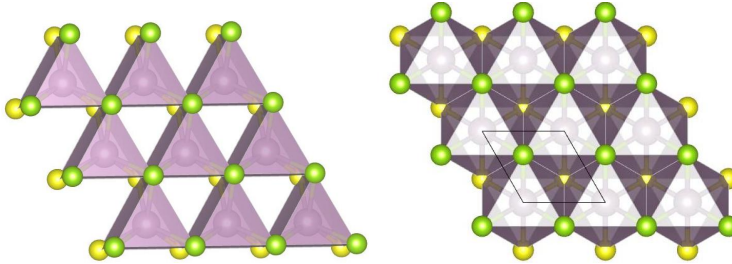

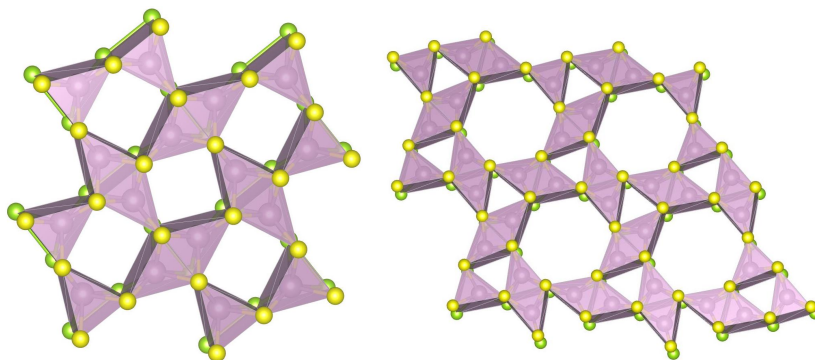Figure 1: Packing of trigonal prisms and octahedra in H and T structures

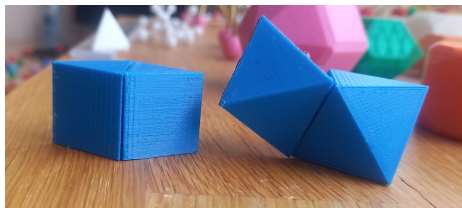Figure 2: Packing of trigonal prisms in fes and fxt structures.

Figure 3: Two face-shared trigonal prisms and octahedra, the diviation from the horisontal plane in the last case is clearly visible

2.2 The new crystal structures

2.2.1 Structures with trigonal prismatic coordination

To compare topologies of H, fes, and fxt structures and produce similar structures with trigonal prismatic coordination, we present the structures as different fillings of the hexagonal net of sulphur atoms (Figure 4). H-structure presents the most symmetric chess-board-like filling. The fes structure can be also considered as the chess-board filling, but with doubled triangular cell, having the form of rhombuses. After optimisation these rhombuses trasforms in the right squares. In fxt structure the non-filled loops are of two types. The first are three doubled triangular (rhombuses) connected through the faces, having the form of right hexagons. The second are primitive triangles. The optimisation does not sufficiently change the form of the non-filled loops, only slightly deforming hexagons.

Three new structures were produced by means of the filling of triangles in the hexagonal net of the sulphur atoms. We name them abstractly test1, test2, and test3. We failed to produce new structures obeying the local charge balance, i.e. the structures in which each vertex of the trigonal prism would be common for two other prisms. In the structure test1, each sulphur atom is common for

two or four filled prisms, in test2 and test3 − for 2, 3, and 4 (Figure 4). Test3 structure is different from the other structures in that it characterised by the presence of trigonal prisms with two common faces, while in all other structures prisms has no more than one common face. Optimisation of test3 structure sufficiently affect the arrangement of sulphur atoms. In the final structure the net of sulphur atoms is not more the hexagonal one.

Presense of common edges and faces of [MoO6] trigonal prisms in fxt, fes, test1, test2, and test3 structure results in shorter Mo–Mo distances in comparison with 1H structure, where prisms have only common edges. In H structure, Mo atoms form regular hexagonal net with all Mo–Mo bonds being equal to 3.25 Å. In fxt, fes, test1, test2, and test3 structures Mo–Mo distances varie in some range, with formation of Mo–Mo dimer connected by the stronger bonds. In optimised H structure, the Mo–Mo bonds distances are equal to 3.25 Å, in H-hor it reaches 3.08 Å, in test1 − 2.9 Å, in fxt, fes, and test2 − in average 2.62 Å, and test3 is characterised by the shortest Mo–Mo distance of 2.22 Ålength. The dimers are in turn connected in chains and layers by the weaker bonds.

Comment. fxt structure was considered as grain-boundary structure of H structure. Similarly we can describe test-1 and test-2 structure, as structures forming at grain boundary forming at contact of grains growing in oppoiste direction (horizontal direction on the figure). Comment. Considering the fact that the total energies of the H phase are comparable to those of the T phase it is reasonable to expect that our proposed H structure could be found at least with the same probability as the T configuration.
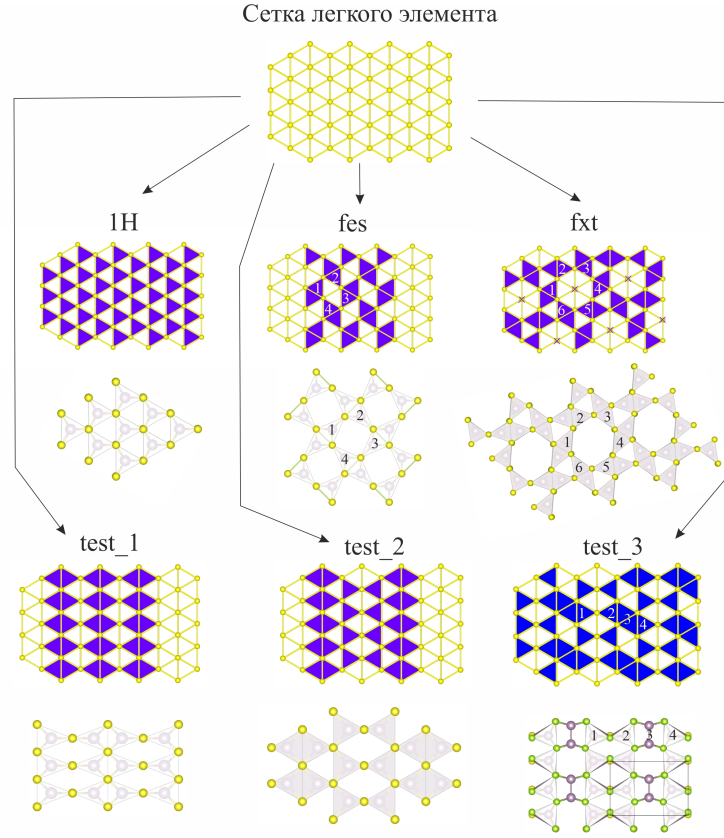
Figure 4: The initial and optimised structures of MoSSe. Тут нужно убрать связь Мо-Мо для test3 и вомзможно показать Мо3 в профиль

Another structure chracterising by trigonal prismatic coordination was found by means of USPEX code. It is sufficiently different from all the considered above structures in that three-fold axes of trigonal prisms are parallel to the place of sulphur atoms. As the result the loops of the net sulphur atoms is not more hexagonal, but square. This structure was called H-hor (from H-horisontal)

2.2.2 Structures with octahedral coordination

As it was mentioned above T structure, composed of closely packed octahedra does not give such a flexibility as H-structure, as contact of octahedra through the face results in the corrugation of the plane of sulphur atoms. One such a structure with face-shared octahedra have been found with AIRSS code. In this structure each octahedra have four common edges and one common face. The presence of the common face results in the sufficient corrugation of the layers of sulphur, in contrast to earlier considered structures. This structure was called
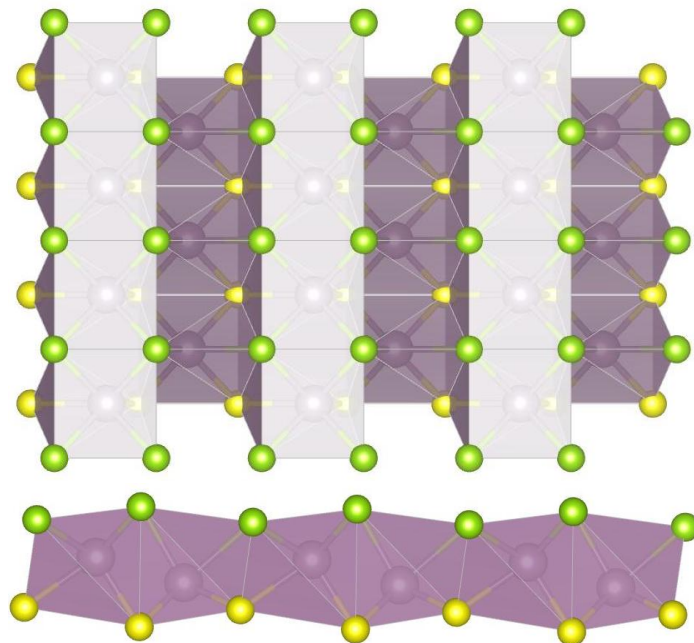
T-hor.

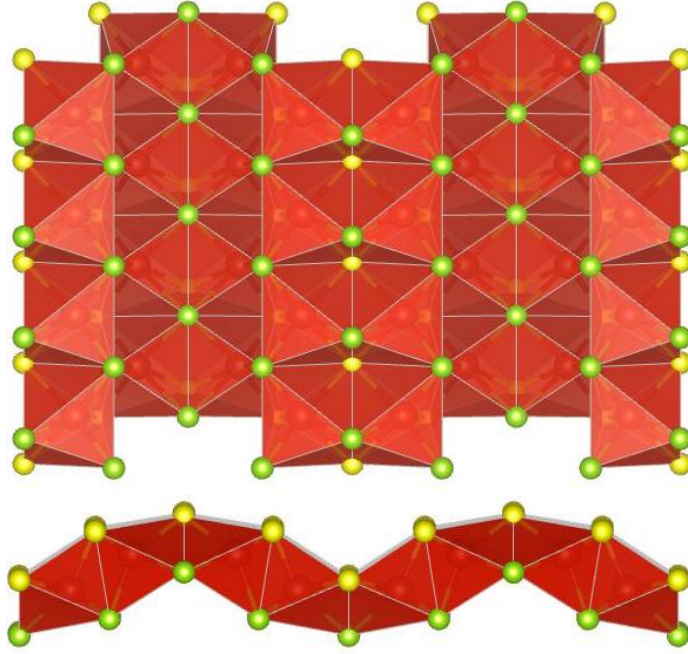Figure 5: H-hor crystal structure perpendicular and along the layer.

Figure 6: T-hor crystal structure perpendicular and along the layer.

2.2.3 5-coordinated crystal structure

Crystal structure with 5-coordinated Mo atoms were revealed with AIRSS code and have been called airss-1. This structure have not analogues with any structures described above. Mo atoms are surrounded by 5 chacogenes arranged in tetragonal or ditrigonal pyramids. Two tetragonal pyramids and one ditrigonal pyramid connected through the edges are grouped in cluters. The adjacent clusters are connected through the common edges. Between clusters there are big holes, the sizes of which are comparable with the sizes of the clusters itself.
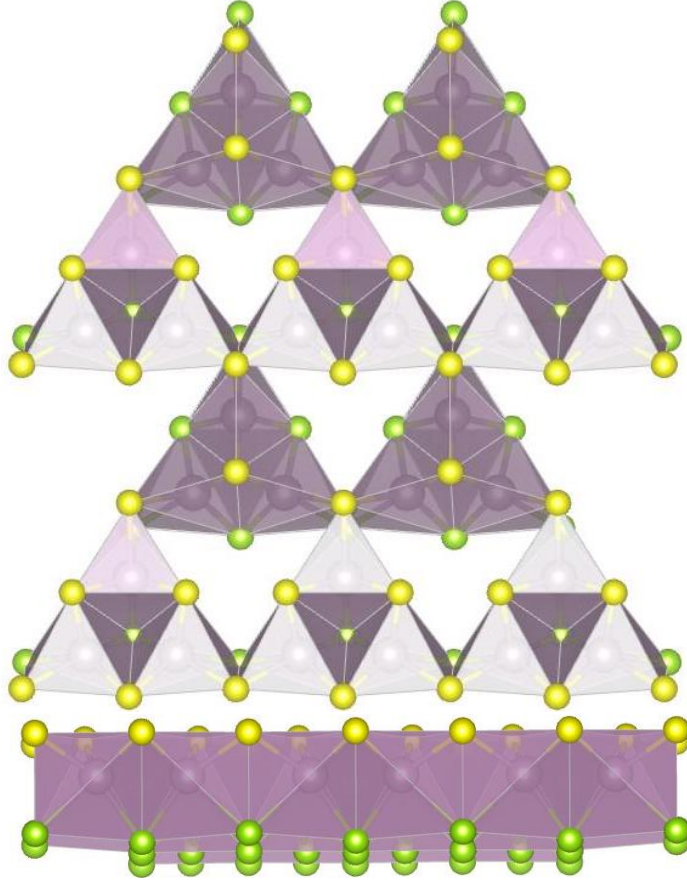
Figure 7: AIRSS-1 structure with 5-coordinated Mo atoms perpendicular and along the layer.

2.2.4 Crystal structure consisting of mixed layers of TM and Ch (chalcogene)

The structure in which TM are sufficiently shifted from the center towards upper and bottom layer was revealed for SVSe composition with AIRSS code and have been called airss-3. V atoms in this structure are characterised by the coordination numbers of five and six, and coordination polyhedron have the forms of tetragonal pyramid and trigonal prism respectively. Structure can be presented as the combination of double chains, one is with the subhorisontal faces of [SV4] composition in the upper layer and another is with subhorisontal faces of [SeV4] composition in the bottom layer. Polyhedrons are connected through the common edges. Each tetragonal pyramid share six out of eight common faces and trigonal pyramid – three out of nein.
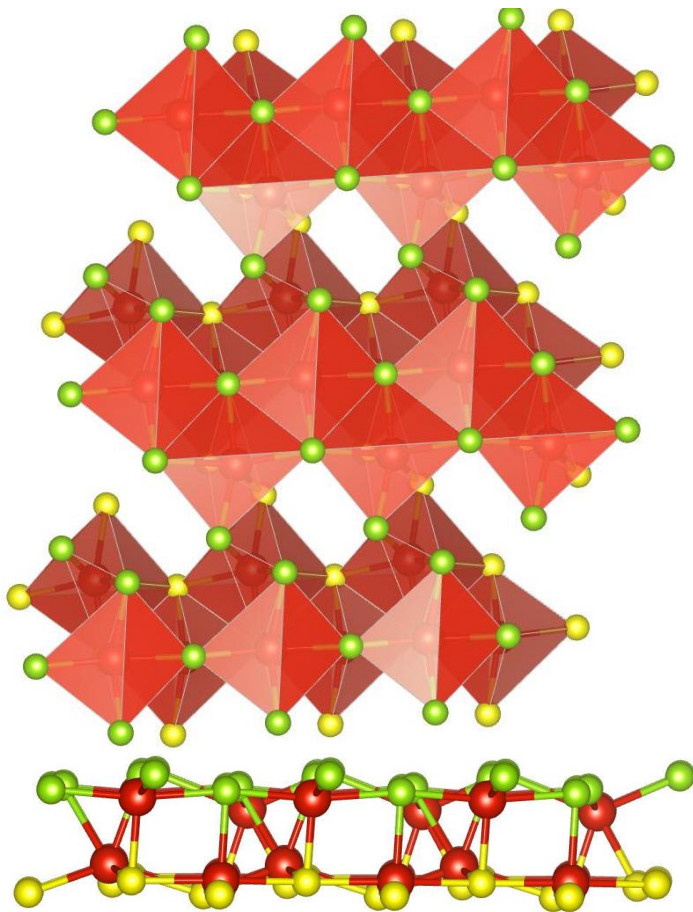
Figure 8: AIRSS-3 structure with V atoms shifted towards the planes of chalcogenes.

2.2.5 The uniquenes of the new structures

To answer the question, whether the found structures are unique or there are similar representatives in ICSD we have performed topological search. The obtained results have shown that all the found structures, except of H-hor, are unique and similar structures are not found in ICSD. The same is true about the earlier known fxt and fes structures, similar structures of which have not also been found. The H-hor structure belong to the same kgd topological type as the T structure. This means that one structure can be transformed into another without breaking the bonds. However the geometrical difference of H-hor and T structures is sufficient and transformation of one structure into the other requires changing of the coordination polyhedron from trigonal prism to octahedron.

Comment: Although TOPOS have not found such a structures, some analogues exist. Interestingly, we note that this structure resembles the structure of the recent experimentally identified monolayer C2N-h2D[J. Mahmood, E. K. Lee, M. Jung, D. Shin, I. Jeon, S. Jung, H. Choi, J. Seo, S. Bae, S. Sohn, N. Park, J. H. Oh, H. Shin, and J. Baek, Nat. Commun. 6, 6486 (2015)]

2.3 Stability of the predicted structures

Table 1: Calculated enthalpies of SMoSe and SVSe structures.

| Phase	Enthalpy (eV/f.u.)		Relative H (eV/f.u.)	
	SMoSe	SVSe	SMoSe	SVSe
1H	-20.8588	-15.7908	0.0000	0.2022
1T	-20.1229	-15.8817	0.7358	0.1113
1T'	-20.4272	-15.9930	0.4315	0.0000
fes	-20.0677	-15.3545	0.7910	0.6385
fxt	-20.0572	-15.2915	0.8016	0.7015
test-1	-19.7876	-15.2359	1.0711	0.7571
test-2	-20.2611	-15.4713	0.5977	0.5217
test-3	-19.9359	-15.5461	0.9229	0.4468
H-hor	-20.0648	-15.7256	0.7939	0.2674
T-hor	-20.3004	-15.9091	0.5584	0.0838
airss-1	-20.2308	-15.6641	0.6280	0.3289
airss-3	-19.6106	-15.6467	1.2481	0.3463
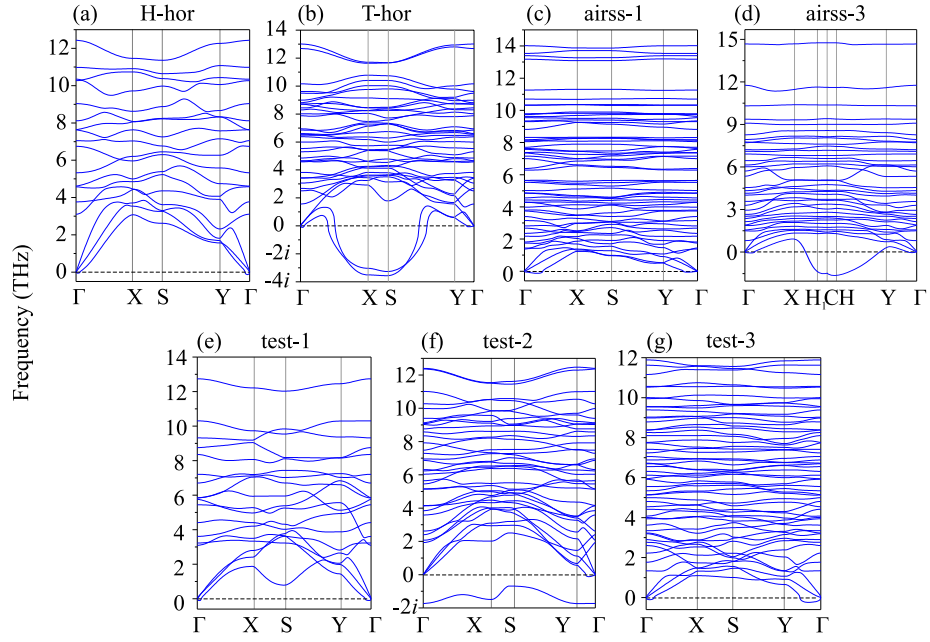
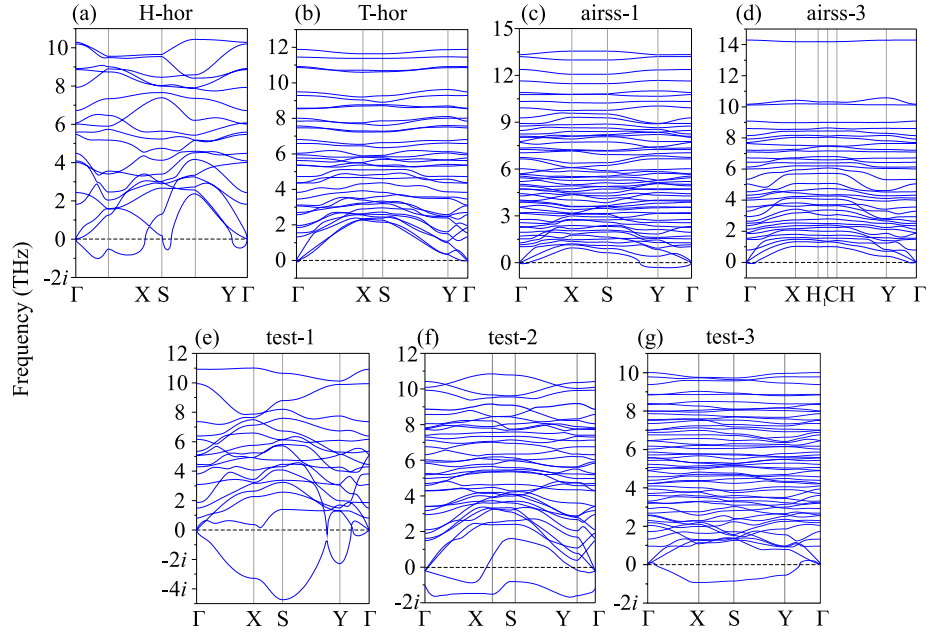Figure 9: Phonon dispersion curves of SMoSe structures.

Figure 10: Phonon dispersion curves of SVSe structures.

2.4 Crystal field splitting

The crystal field theory proceeds from the fact that the nature of ligands and their location around the central ion (symmetry of the complex) reduce the degeneracy of d-orbitals and change their energy. As all investigated structures consist of transition metal atoms surrounded by ligands (chalcogen atoms), the presence of the ligands splits the d-electrons levels depending on local symmetry. Thereby the correlation between structure and electronic properties can be interpreted in terms of crystal field theory. According to crystal field theory, in an octahedral environment (1T polymorph), the d-shell splits into a low-energy triplet (t2g) and a high-energy doublet (eg). In a trigonal prismatic geometry (1H), the low-energy triplet further splits into a doublet and a singlet [https://doi.org/10.1088/2053-1583/ab0188]. The two polymorphs of MoS2 have distinct electronic properties, the 1H-MoS2 is a semiconductor and the 1T-MoS2 is metallic. The fes-MoSSe despite the prismatic environment of TM atom becomes a semi-metal [10.1016/j.physe.2020.114485 , 10.1039/D1NA00112D] and fxt Mo and W based TMDs are gapless semiconductors or, alternatively, semimetals [10.1103/PhysRevB.93.035442].

3 Conclusions

The variation of structures dictates variation electronic properties based on different d-splitting and electron filling of d-orbitals which makes it possible to manipulate electronic properties through phase transformation.

References

[1] Zhang, Q.; Mei, L.; Cao, X.; Tang, Y.; Zeng, Z. Intercalation and exfoliation chemistries of transition metal dichalcogenides. *Journal of Materials Chemistry A 8*, **2020**, 15417–15444.

[2] Li, X.; Tao, L.; Chen, Z.; Fang, H.; Li, X.; Wang, X.; Xu, J.-B.; Zhu, H. Graphene and related two-dimensional materials: Structure-property relationships for electronics and optoelectronics. *Applied Physics Reviews 4*, **2017**, 021306.

[3] Shi, J.; Hong, M.; Zhang, Z.; Ji, Q.; Zhang, Y. Physical properties and potential applications of two-dimensional metallic transition metal dichalcogenides. *Coordination Chemistry Reviews 376*, **2018**, 1–19.

[4] Xi, X.; Wang, Z.; Zhao, W.; Park, J.-H.; Law, K. T.; Berger, H.; Forró, L.; Shan, J.; Mak, K. F. Ising pairing in superconducting nbse 2 atomic layers. *Nature Physics 12*, **2016**, 139–143.

[5] Hu, H.; Zavabeti, A.; Quan, H.; Zhu, W.; Wei, H.; Chen, D.; Ou, J. Z. Recent advances in two-dimensional transition metal dichalcogenides for biological sensing. *Biosensors and Bioelectronics 142*, **2019**, 111573.

[6] Pi, L.; Li, L.; Liu, K.; Zhang, Q.; Li, H.; Zhai, T. Recent progress on 2d noble-transition-metal dichalcogenides. *Advanced Functional Materials 29*, **2019**, 1904932.

[7] Nayeri, M.; Moradinasab, M.; Fathipour, M. The transport and optical sensing properties of mos2, mose2, ws2 and wse2 semiconducting transition metal dichalcogenides. *Semiconductor Science and Technology 33*, **2018**, 025002.

[8] Zhao, B.; Shen, D.; Zhang, Z.; Lu, P.; Hossain, M.; Li, J.; Li, B.; Duan, X. 2d metallic transition-metal dichalcogenides: Structures, synthesis, properties, and applications. *Advanced Functional Materials 31*, **2021**, 2105132.

[9] Xu, H.; Wei, J.; Zhou, H.; Feng, J.; Xu, T.; Du, H.; He, C.; Huang, Y.; Zhang, J.; Liu, Y.; et al. High spin hall conductivity in large-area type-ii dirac semimetal ptte2. *Advanced Materials 32*, **2020**, 2000513.

[10] Zhao, B.; Khokhriakov, D.; Zhang, Y.; Fu, H.; Karpiak, B.; Hoque, A. M.; Xu, X.; Jiang, Y.; Yan, B.; Dash, S. P. Observation of charge to spin conversion in weyl semimetal wte 2 at room temperature. *Physical Review Research 2*, **2020**, 013286.

[11] Wang, L.; Fang, Y.; Huang, Y.; Cheng, E.; Ni, J.; Pan, B.; Xu, Y.; Huang, F.; Li, S. Nodeless superconducting gap in the topological superconductor candidate 2 m–ws 2. *Physical Review B 102*, **2020**, 024523.

[12] Hsu, Y.-T.; Vaezi, A.; Fischer, M. H.; Kim, E.-A. Topological superconductivity in monolayer transition metal dichalcogenides. *Nature communications 8*, **2017**, 1–6.

[13] Huang, H.; Fan, X.; Singh, D. J.; Zheng, W. Recent progress of tmd nanomaterials: phase transitions and applications. *Nanoscale 12*, **2020**, 1247–1268.

[14] Ataca, C.; Sahin, H.; Ciraci, S. Stable, single-layer mx2 transition-metal oxides and dichalcogenides in a honeycomb-like structure. *The Journal of Physical Chemistry C 116*, **2012**, 8983–8999.

[15] Kan, M.; Wang, J.; Li, X.; Zhang, S.; Li, Y.; Kawazoe, Y.; Sun, Q.; Jena, P. Structures and phase transition of a mos2 monolayer. *The Journal of Physical Chemistry C 118*, **2014**, 1515–1522.

[16] Wang, X.; Shen, X.; Wang, Z.; Yu, R.; Chen, L. Atomic-scale clarification of structural transition of mos2 upon sodium intercalation. *ACS nano 8*, **2014**, 11394–11400.

[17] Duerloo, K.-A. N.; Li, Y.; Reed, E. J. Structural phase transitions in two-dimensional mo-and w-dichalcogenide monolayers. *Nature communications 5*, **2014**, 1–9.

[18] Tang, Q.; Jiang, D.-e. Stabilization and band-gap tuning of the 1t-mos2 monolayer by covalent functionalization. *Chemistry of Materials 27*, **2015**, 3743–3748.

[19] Voiry, D.; Goswami, A.; Kappera, R.; e Silva, C. d. C. C.; Kaplan, D.; Fujita, T.; Chen, M.; Asefa, T.; Chhowalla, M. Covalent functionalization of monolayered transition metal dichalcogenides by phase engineering. *Nature chemistry 7*, **2015**, 45–49.

[20] Murphy, D. W.; Cros, C.; Di Salvo, F. J.; Waszczak, J. Preparation and properties of lixvs2 (0. ltoreq. x. ltoreq. 1). *Inorganic Chemistry 16*, **1977**, 3027–3031.

[21] Le Nagard, N.; Katty, A.; Collin, G.; Gorochov, O.; Willig, A. Elaboration, structure cristalline et proprietes physiques (transport, susceptibilité magnétique et rmn) du spinelle cuv2s4. *Journal of Solid State Chemistry 27*, **1979**, 267–277.

[22] Lu, A.-Y.; Zhu, H.; Xiao, J.; Chuu, C.-P.; Han, Y.; Chiu, M.-H.; Cheng, C.-C.; Yang, C.-W.; Wei, K.-H.; Yang, Y.; et al. Janus monolayers of transition metal dichalcogenides. *Nature nanotechnology 12*, **2017**, 744–749.

[23] Zhang, J.; Jia, S.; Kholmanov, I.; Dong, L.; Er, D.; Chen, W.; Guo, H.; Jin, Z.; Shenoy, V. B.; Shi, L.; et al. Janus monolayer transition-metal dichalcogenides. *ACS nano 11*, **2017**, 8192–8198.

[24] Li, F.; Wei, W.; Zhao, P.; Huang, B.; Dai, Y. Electronic and optical properties of pristine and vertical and lateral heterostructures of janus mosse and wsse. *The journal of physical chemistry letters 8*, **2017**, 5959–5965.

[25] Van Thanh, V.; Van, N. D.; Saito, R.; Hung, N. T.; et al. First-principles study of mechanical, electronic and optical properties of janus structure in transition metal dichalcogenides. *Applied Surface Science 526*, **2020**, 146730.

[26] Hu, T.; Jia, F.; Zhao, G.; Wu, J.; Stroppa, A.; Ren, W. Intrinsic and anisotropic rashba spin splitting in janus transition-metal dichalcogenide monolayers. *Physical Review B 97*, **2018**, 235404.

[27] Dong, L.; Lou, J.; Shenoy, V. B. Large in-plane and vertical piezoelectricity in janus transition metal dichalchogenides. *ACS nano 11*, **2017**, 8242–8248.

[28] Li, R.; Cheng, Y.; Huang, W. Recent progress of janus 2d transition metal chalcogenides: from theory to experiments. *Small 14*, **2018**, 1802091.

[29] Xia, C.; Xiong, W.; Du, J.; Wang, T.; Peng, Y.; Li, J. Universality of electronic characteristics and photocatalyst applications in the two-dimensional janus transition metal dichalcogenides. *Physical Review B 98*, **2018**, 165424.

[30] Ma, X.; Wu, X.; Wang, H.; Wang, Y. A janus mosse monolayer: a potential wide solar-spectrum water-splitting photocatalyst with a low carrier recombination rate. *Journal of Materials Chemistry A 6*, **2018**, 2295–2301.

[31] Er, D.; Ye, H.; Frey, N. C.; Kumar, H.; Lou, J.; Shenoy, V. B. Prediction of enhanced catalytic activity for hydrogen evolution reaction in janus transition metal dichalcogenides. *Nano letters 18*, **2018**, 3943–3949.

[32] Zhou, Z.; Niu, X.; Zhang, Y.; Wang, J. Janus mosse/wsete heterostructures: a direct z-scheme photocatalyst for hydrogen evolution. *Journal of Materials Chemistry A 7*, **2019**, 21835–21842.

[33] Oganov, A. R.; Glass, C. W. Crystal structure prediction using ab initio evolutionary techniques: Principles and applications. *The Journal of Chemical Physics 124*, **2006**, 244704.

[34] Oganov, A. R.; Lyakhov, A. O.; Valle, M. How evolutionary crystal structure prediction works—and why. *Accounts of Chemical Research 44*, **2011**, 227–237.

[35] Lyakhov, A. O.; Oganov, A. R.; Stokes, H. T.; Zhu, Q. New developments in evolutionary structure prediction algorithm uspex. *Computer Physics Communications 184*, **2013**, 1172–1182.

[36] Pickard, C. J.; Needs, R. J. High-pressure phases of silane. *Physical Review Letters 97*, **2006**, 045504.

[37] Pickard, C. J.; Needs, R. J. Ab initio random structure searching. *Journal of Physics: Condensed Matter 23*, **2011**, 053201.

[38] Blöchl, P. E. Projector augmented-wave method. *Physical review B 50*, **1994**, 17953.

[39] Kresse, G.; Furthmüller, J. Efficient iterative schemes for ab initio total-energy calculations using a plane-wave basis set. *Physical Review B 54*, **1996**, 11169–11186.

[40] Kresse, G.; Furthmüller, J. Efficiency of ab-initio total energy calculations for metals and semiconductors using a plane-wave basis set. *Computational Materials Science 6*, **1996**, 15–50.

[41] Perdew, J. P.; Burke, K.; Ernzerhof, M. Generalized gradient approximation made simple. *Physical Review Letters 77*, **1996**, 3865.

[42] Monkhorst, H. J.; Pack, J. D. Special points for brillouin-zone integrations. *Physical review B 13*, **1976**, 5188.

[43] Togo, A.; Tanaka, I. First principles phonon calculations in materials science. *Scripta Materialia 108*, **2015**, 1–5.

[44] Momma, K.; Izumi, F. Vesta 3 for three-dimensional visualization of crystal, volumetric and morphology data. *Journal of applied crystallography 44*, **2011**, 1272–1276.